Human Molecular Genetics, 2001, Vol. 10, No. 3 211–219

The spatial organization of human chromosomes within the nuclei of normal and emerin-mutant cells

Shelagh Boyle[1], Susan Gilchrist[1], Joanna M. Bridger[1,+], Nicola L. Mahy[1], Juliet A. Ellis[2] and Wendy A. Bickmore[1,§]

[1]MRC Human Genetics Unit, Crewe Road, Edinburgh EH4 2XU, UK and [2]Randall Centre for the Molecular Mechanism of Cell Function, King's College, Guy's Campus, London SE1 1UL, UK

Received 7 October 2000; Revised and Accepted 27 November 2000

To fully understand genome function, the linear genome map must be integrated with a spatial map of chromosomes in the nucleus. Distinct nuclear addresses for a few human chromosomes have been described. Previously we have demonstrated that the gene-rich human chromosome 19 is located in a more central position in the nucleus than the similarly sized, but gene-poor, chromosome 18. To determine whether these two chromosomes are a paradigm for the organization of chromatin in the human nucleus, we have now analysed the nuclear organization of every human chromosome in diploid lymphoblasts and primary fibroblasts. We find that the most gene-rich chromosomes concentrate at the centre of the nucleus, whereas the more gene-poor chromosomes are located towards the nuclear periphery. In contrast, we find no significant relationship between chromosome size and position within the nucleus. Proteins of the nuclear membrane or lamina are candidates for molecules that might anchor regions of the genome at the nuclear periphery and it has been suggested that disruption of this organization may play a role in some disease pathologies. We show that the intranuclear organization of chromosomes is not altered in cells that lack the integral nuclear membrane protein emerin, from an individual with X-linked Emery–Dreifuss muscular dystrophy. This suggests that emerin is not necessary for localizing chromosomes at the nuclear periphery and that the muscular dystrophy phenotype in such individuals is not due to grossly altered nuclear organization of chromatin.

INTRODUCTION

Large numbers of genes have now been mapped to different human chromosomes (1) and the DNA sequences of two human chromosomes have been published (2,3). However, spatial organization within the mammalian nucleus can influence gene expression (4,5) and in model organisms the nuclear periphery is a site of transcriptional inactivity and gene repression (6). Hence, levels of human genome organization beyond the primary DNA sequence need to be investigated. Previously we have shown that the territories of human chromosomes 18 and 19 (HSA18 and -19) are located in different compartments of the nucleus. The gene-rich chromosome HSA19 was found in the centre of the nucleus, whereas gene-poor HSA18 is situated at the nuclear periphery (7). This suggested that there might be a general organization within the human nucleus in which chromosomes with the highest gene concentration are sequestered to the centre of the nucleus and more inactive chromatin is at the nuclear periphery. Alternatively, HSA18 and -19 might be unusual in their nuclear location and have no general bearing on the organization of the human nucleus. To test these hypotheses we have now analysed the spatial organization of the entire human chromosome set in the nuclei of diploid primary and transformed cells of normal individuals. We show that there is a correlation between the estimated gene density of each chromosome and its average position within the nucleus, but we find no statistically significant relationship between chromosome size and nuclear position. Human chromosomes that we measure as being in closest proximity to the nuclear periphery are generally considered to be gene-poor. The most gene-rich human chromosomes concentrate towards the centre of the nucleus.

Factors that mediate the nuclear positioning of individual chromosomes are not known. However, interactions among components of the nuclear membrane, nuclear lamina and chromatin are thought to be important in establishing or maintaining nuclear architecture (8). X-linked Emery–Dreifuss muscular dystrophy (X-EDMD) is caused by mutations in the gene encoding emerin. Emerin is a ubiquitous type II integral membrane protein localized to the inner nuclear membrane and most X-EDMD-associated mutations result in a loss of emerin protein at the membrane (7–9). The mechanistic links between loss of emerin function and the muscular dystrophy phenotype (cardiac conduction defects, early contractures and progressive wasting of specific sets of muscles) are not clear. Differentiated striated muscle cells are non-dividing and long-lived and therefore the nuclear membrane has to maintain structural integrity over a long time. One suggestion is that the disease results because loss of mechanical strength of the nuclear membrane causes nuclear fragility during muscle contraction

[+]Present address: Department of Biological Sciences, Brunel University, Uxbridge, Middlesex UB8 3PH, UK
[§]To whom correspondence should be addressed. Tel: +44 131 332 2471; Fax: +44 131 343 2620; Email: w.bickmore@hgu.mrc.ac.uk

(10). However, it has also been argued that disease pathology might be caused by altered nuclear organization, in particular by an inability to sequester inactive chromatin to the nuclear periphery (11), leading to disregulated gene expression. Here we show that the positioning of gene-poor chromosomes at the nuclear periphery is not grossly perturbed in cells lacking emerin protein. This suggests that emerin is not necessary for the localization of large blocks of gene-poor chromatin at the nuclear periphery of human cells and argues against EDMD being a disease of altered chromatin organization that leads to aberrant gene expression.

RESULTS

The relationship between estimated gene density and chromosome position in the nuclei of human lymphoblasts

To determine the intranuclear organization of the entire human karyotype, chromosome paints for each chromosome were first used in fluorescence *in situ* hybridization (FISH) to male lymphoblast nuclei fixed in methanol/acetic acid (MAA) (Fig. 1) (7,12). Analysis of two-dimensional images is efficient and can be automated so that large numbers of nuclei can be scored (7). In addition, plane projections can be used to make inferences about three-dimensional objects (13). To determine the relative nuclear position of each chromosome we measured distances between the centroid (signal intensity weighted centre) of the chromosome territory and both the edge and centroid of the nucleus (7). When these values are plotted against the estimated gene density of each chromosome (1) a significant correlation emerges (Fig. 2A). The human chromosomes (HSA4, -5, -8, -13 and -18) with observed/expected ratios of gene markers that are significantly < 1 (1) are those whose centroids are close to the nuclear periphery (small distance to the edge, large distance to the centre of the nucleus). The centroids of chromosomes significantly enriched in gene-based markers (HSA1, -17, -19 and -22) are located far from the edge of the nucleus and close to the nuclear centre (Fig. 2A). Linear regression confirms the significance of the relationship between gene density and nuclear position (Fig. 2), but highlights chromosome 11 and 16 measurements as having large standardized residuals. We found HSA16 towards the centre of the nucleus (Fig. 2), even though its reported expressed sequence tag (EST) density is low (1). However, HSA16 is enriched in other features indicative of high gene concentration: CpG islands (14), the most GC-rich isochores (15) and hyperacetylated histones (16). All of these lines of evidence point towards EST analysis as having significantly underestimated the true gene density of HSA16. Similarly, the distribution of CpG islands, GC-rich DNA and hyperacetylated histones suggests that HSA11 is not an especially gene-rich chromosome and it is not disposed with the other gene-rich chromosomes towards the centre of the nucleus. For other human chromosomes the estimated gene density calculated from EST mapping (1) generally accords with the other, less quantifiable, indicators of gene concentration discussed above.

Linear regression of the data in Figure 2B shows that there is no simple significant correlation between physical chromosome size (17) and nuclear position. It is also clear, from our previous analysis of HSA18 and -19 and from the data in Figure 1, that human chromosomes of similar physical size but different functional characteristics adopt different nuclear positions.

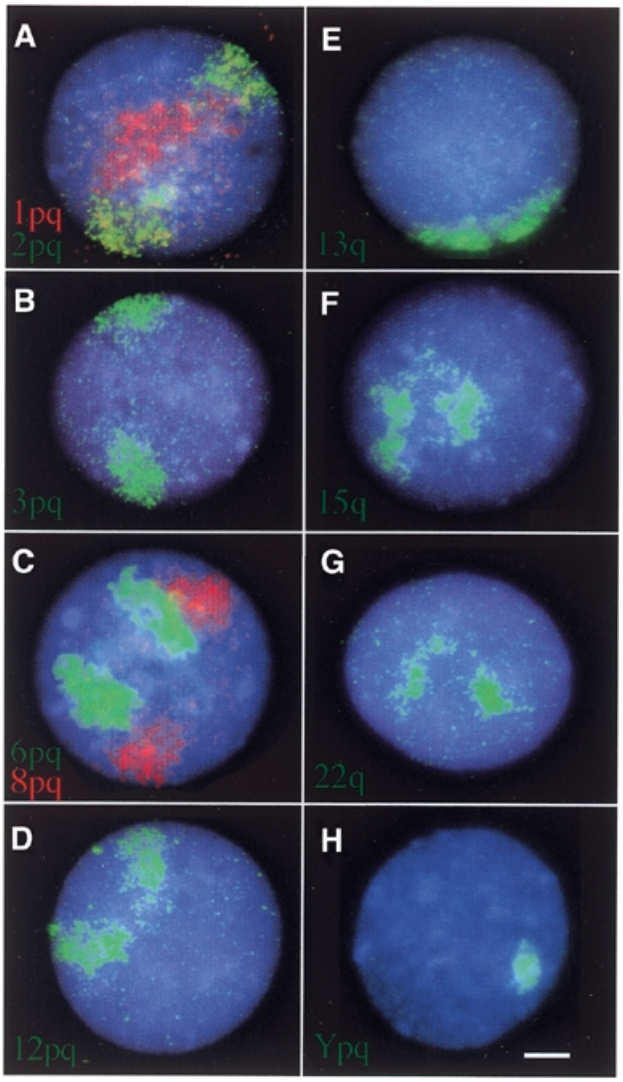

Figure 1. The position of selected chromosome territories in normal human lymphoblast nuclei. Hybridization of MAA-fixed human 46,XY lymphoblast nuclei with chromosome paints for HSA1, -2, -3, -6, -8, -12, -13, -15, -22 and Y. All nuclei were counterstained with DAPI (blue) and chromosome territories were detected in either green or red as indicated. For HSA13, -15 and -22 only q arm probes were used to avoid cross-hybridization between shared p arm sequences. Bar, 2 μm.

Mean chromosome position was also analysed from the distribution of hybridization signal across five concentric shells eroded from the periphery of lymphoblast nuclei to the centre (Fig. 3) (7,12). This allows the nuclear distribution of the entire bulk chromosome territory to be assessed, not only the territory centre as in Figure 2. However, consistent with the analysis in Figure 2, the chromosomes for which the hybridization signal is significantly concentrated towards the centre of the nucleus (signal shell 5 > shell 1, $P < 0.005$) are HSA1, -16, -17, -19 and -22 (Fig. 3). We consider all of these chromosomes to be significantly enriched in genes and active chromatin (1,14–16). Chromosome territories with a similarly

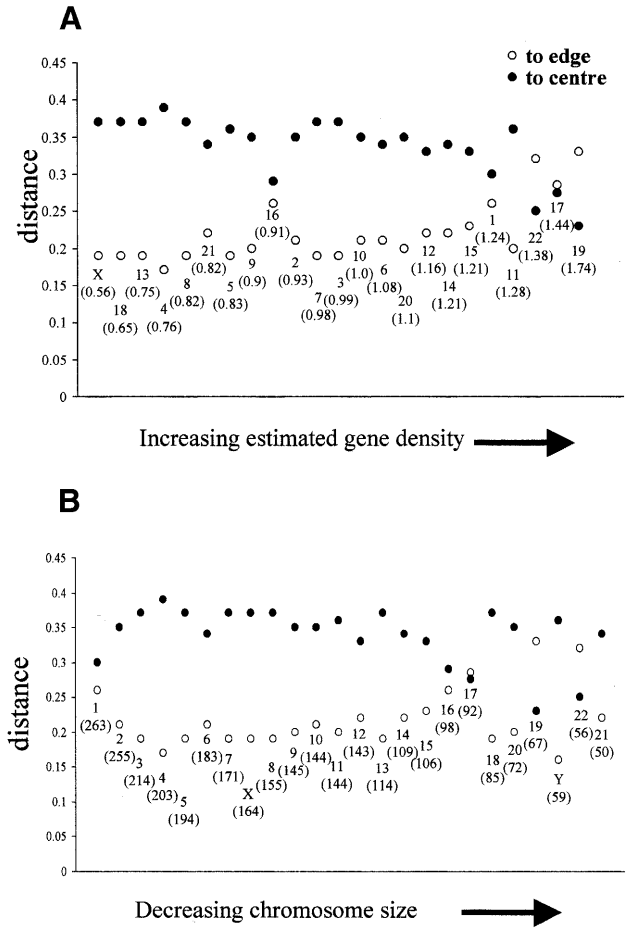

Figure 2. Relationship of estimated gene density or size and chromosome position within the human nucleus. Graphs show the mean distance (in pixels) normalized for nuclear size [divided by (nuclear radius)^2] between the centroid of chromosome territories and the edge (open circles) or centroid (closed circles) of 50 MAA-fixed lymphoblast nuclei each. All standard errors of the mean were ≤0.01. In (**A**) the chromosomes are arranged along the *x*-axis in order of increasing predicted gene density according to the observed/expected ratio of ESTs (not available for the human Y chromosome) (1). This ratio is shown in parentheses below the chromosome number. In (**B**) the chromosomes are ordered in decreasing physical size (17). The size in Mb is shown in parentheses below the chromosome number. Linear regression shows a significant correlation between estimated gene density and the distance from either the edge ($r^2 = 55.8\%$, $P = 0.000$) or centre ($r^2 = 61.2\%$, $P = 0.000$) of the nucleus (A). (B) Regression indicates that there is not a significant correlation between chromosome size and proximity to either the edge ($r^2 = 23.8\%$, $P = 0.02$) or the centre ($r^2 = 12.4\%$, $P = 0.1$) of the nucleus.

significant enrichment towards the nuclear periphery (shell 1 > shell 5, $P < 0.005$) are HSA2, -3, -4, -7, -8, -11, -13 and -18 (Fig. 3). Chromosomes with less significant ($P < 0.06$) enrichment towards the nuclear periphery include the X and Y in these male cells and HSA9, -12 and -20. Signals from HSA5, -6, -10, -14, -15, -20 and -21 have no significant bias to either the most peripheral or central shells.

Analysing chromosome position in primary fibroblasts and in three-dimensionally preserved nuclei

Erosion analysis is also applicable to cells in which the nuclei are not circular/spherical. Previously we found that HSA18 and -19 have the same differential distribution in the elliptical nuclei of proliferating skin fibroblasts as in the spherical nuclei typical of lymphoblasts (12). This suggested that nuclei in these two cell types are organized with similar principles despite their different overall shape. When the position of other chromosomes was analysed in primary male fibroblast nuclei fixed with MAA, the same propensity of signals from gene-rich chromosomes to concentrate in the nuclear interior was seen. HSA1, -16, -17, -19 and -22 were significantly enriched in the central nuclear shell (shell 5 > shell 1, $P \leq 0.03$). As in lymphoblasts, HSA2, -13 and -18 were enriched at the nuclear periphery (shell 1 > shell 5, $P \leq 0.03$) (Fig. 4). This suggests that the organization of chromosomes within human fibroblasts is broadly similar to that in lymphoblasts. However, there were also some notable differences between these two cell types in the way in which signals from some chromosomes were distributed across the eroded nuclear shells. In particular, whereas chromosome 21 was not significantly enriched in the most central nuclear shell of lymphoblasts, it is significantly enriched in the centre of fibroblast nuclei ($P < 0.005$). This may reflect constraints imposed on the position of this small acrocentric chromosome by nucleoli in different cell types. We also did not detect a significant enrichment of signal from chromosome 8 in the most peripheral shell of fibroblast nuclei (signals peak in shell 2). The basis for this difference to lymphoblasts is not understood.

The inactive X chromosome is known to locate at the nuclear periphery in female cells, but the active X has not been similarly analysed (18). Interestingly, we found that both the single (active) X in male human fibroblasts and the two Xs (one active and one inactive) in female fibroblasts were significantly enriched ($P \leq 0.005$) in the most peripheral nuclear shell (Fig. 4). Although many loci have been mapped to the X chromosome because of their pattern of sex-linked inheritance, it is gene-poor (1,14). In an analysis that compared the shapes of active and inactive X chromosome territories, there also did not seem to be large differences in the apparent intranuclear location of the two X chromosomes (19).

The position of chromosomes was also examined in *z* sections at 0.5 μm intervals through the three-dimensionally preserved nuclei of primary fibroblasts fixed with formaldehyde (7,12). We measured the distance between the centre of chromosome territories and the nearest apical or lateral edge of the elliptical nuclei, relative to the radius of the long (*x*) or short (*y*) axes of the nucleus, respectively (Fig. 5). The position of territories relative to the top or bottom surfaces of the nucleus was also examined. For the chromosomes examined, the order of proximity to the apical edge was: 2, X, 1, 13, 17, 6; and to the lateral nuclear edge it was: 2, 13, X, 1, 6, 17 (Fig. 5). This is generally consistent with the observations obtained from two-dimensional analysis, but adds extra information about the relative location of different chromosomes in the nucleus. For example, chromosomes 2 locate close to both the apical and lateral edges of the nucleus (distance between territory centre and edge of the nucleus is 0.47 and 0.42 of the nuclear radius, in the *x* and *y* directions, respectively) (Fig. 5A). However, the territory centres for the q arms of chromosomes 13 are close to the lateral edge of the nucleus (0.45 of the fractional radius), but more distant (0.57) from the apical edge. This may reflect the association of the short arm of this chromosome with the nucleolus (Fig. 5F).

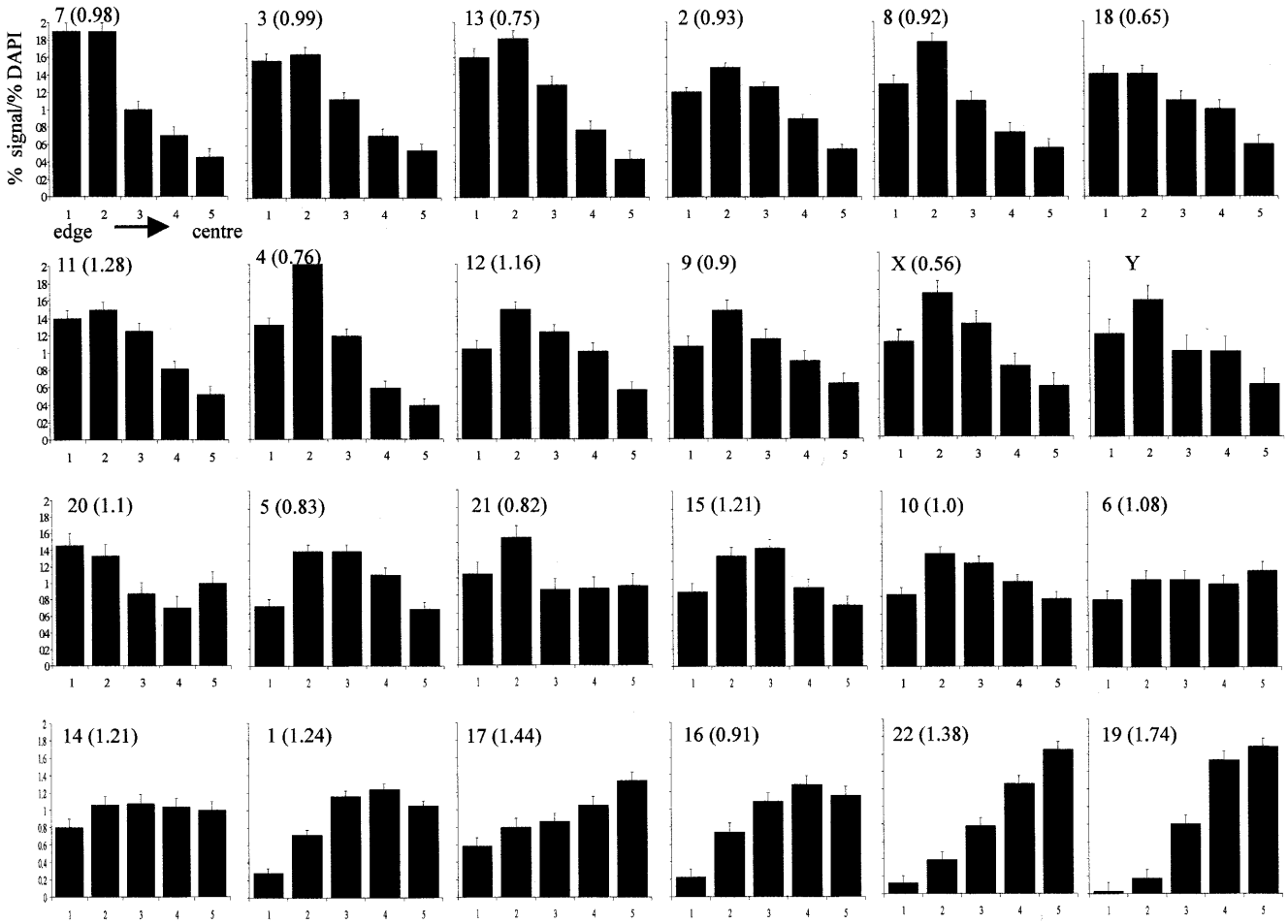

Figure 3. Mean proportion (%) of hybridization signals for each human chromosome, normalized to % DAPI signal, in eroded shells of 46,XY MAA-fixed lymphoblast nuclei. Analysis was by erosion of five concentric shells of equal area from the edge (shell 1) to the centre (shell 5) of 50 nuclei each. Error bars show standard error of the mean. The numbers in parentheses are the observed/expected ratio of gene markers from Deloukas *et al.* (1). Chromosomes are ordered from the top left beginning with those which have a highly significant ($P \leq 0.005$) predomination of hybridization signal in shell 1 over that in shell 5 (HSA7 to -4). Chromosomes 12–20 have a less highly significant enrichment of signal in the outer versus inner nuclear shell ($P = 0.005$–0.06). For chromosomes 5 through 14 there is no significant bias of signal to either the inner or outer shells ($P \geq 0.1$). Lastly, signals from chromosomes 1–19 are significantly ($P \leq 0.02$) enriched in the inner nuclear shell.

Although the p arms of the human rDNA carrying chromosomes HSA13, -14, -15, -21 and -22 are clustered together as nucleoli, our analysis shows that the q arms of these chromosomes can occupy very different nuclear positions. 22q is consistently one of the most centrally located chromosome arms (Figs 1G, 2, 3 and 4) and is rich in both predicted genes and gene markers (1,2,14,20) and other chromosome features associated with gene-rich chromatin (15,16). In contrast, the peripherally located long arm of HSA13 (Figs 1E, 2, 3, 4 and 5) is depleted for ESTs and CpG islands (1,14) and is GC-poor and packaged with hypoacetylated histones (15,16).

The location of chromosomes in the absence of emerin

The factors that determine the intranuclear position of chromosomes are not known. Previously, we showed that inhibiting transcription or histone deacetylation does not perturb the location of HSA18 or -19 in proliferating cells (7). However, chromosome position is not immutable and is established during a narrow time window after nuclear envelope formation in G_1 (12). Several proteins of the nuclear envelope or lamina have chromatin-binding properties and it has been suggested that they play a role in nuclear architecture, especially in sequestering heterochromatin and other regions of silent chromatin to the nuclear periphery (11). To determine whether this is the case, nuclear architecture must be examined in cells mutant for components of the nuclear periphery. X-EDMD is caused by mutations in the integral nuclear membrane protein emerin. We examined the localization of key human chromosomes in lymphoblast cells from an individual with a null mutation in emerin (K2 in ref. 21). No emerin protein is detected in this individual due to a nonsense mutation at the start codon (ATG→ATA) (21). We found that the relative spatial organization of chromosomes in nuclei from this individual was not significantly different to that of normal cells. Gene-poor chromosomes (e.g. HSA4 and -18) were at the nuclear periphery, whereas HSA1 and -17 were in central positions (Fig. 6). The proportion of nuclear area that the chromo-

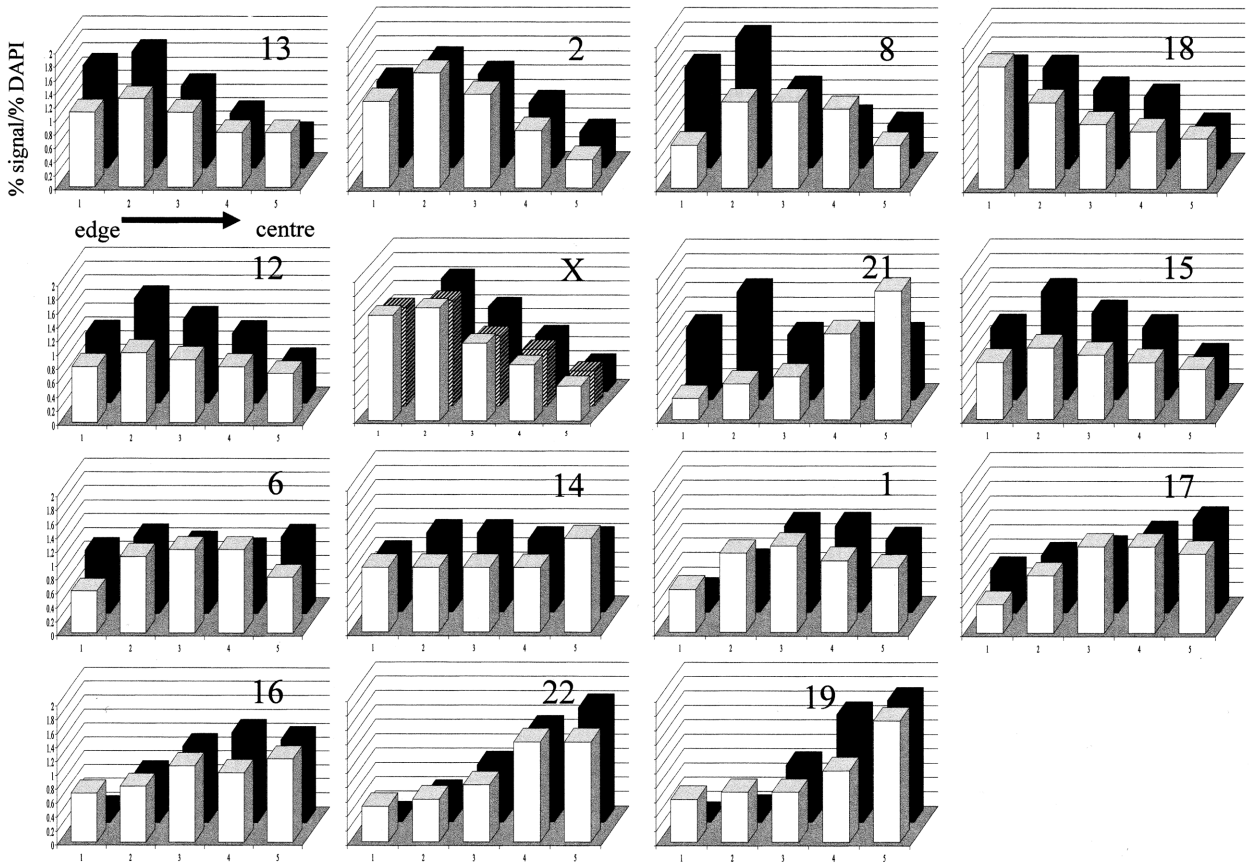

Figure 4. Mean proportion (%) of hybridization signals for selected human chromosomes, normalized to % DAPI stain, in eroded shells of MAA-fixed 46,XY lymphoblast (filled bars) and fibroblast (open bars) nuclei. The X chromosome was analysed in both male (open bars) and female (hatched bars) fibroblasts.

some territories occupied was also the same in normal and X-EDMD cells (data not shown).

DISCUSSION

This is the first attempt to compare the spatial relationships of all the human chromosome territories relative to the interior or periphery of the nucleus. We suggest that the most gene-dense regions of the human genome are preferentially located in the nuclear interior with the gene-poor regions located progressively towards the nuclear periphery. This accords with the clustering in the nuclear interior of the most hyperacetylated, GC-rich and early replicating fractions of the genome (22). The human chromosomes that are consistently concentrated together in the central part of the nucleus are HSA1, -16, -17, -19 and -22 (Figs 2, 3 and 4). In contrast, HSA2, -4, -13 and -18 are some of the most peripherally located chromosomes.

From the analysis of chromosome position within metaphase spreads, it had been suggested that there might be a correlation between chromosome size and nuclear position, with the smallest human chromosomes being confined to the central zone of the nucleus (23–25). This would suggest that simple geometric constraints might dictate nuclear organization. However, our analysis shows that chromosomes of very similar size (17), e.g. HSA17, -18 and -19 or HSA1 and -2 (Figs 1A, 2, 3 and 4) or HSA13 and -14, can be located in quite different positions in the nucleus. Linear regression of the data in Figure 2B confirms that there is no simple correlation between physical chromosome size (bp) and nuclear position. Recently, a relationship between chromosome size and nuclear position was reported (26). However, this analysis only examined the intranuclear position of q arm telomeres for nine chromosomes. It is not clear how telomere position relates to that of the chromosome territory as a whole. For example, we previously found that both telomeres of human chromosome 18 are in a more internal nuclear position than the chromosome arms themselves (7).

We have described the mean position within the nucleus of the bulk chromatin for each human chromosome. However, our analysis does not preclude smaller regions from each chromosome occupying a nuclear location quite distinct from the rest of its host chromosome. For example, it is likely that small late-replicating regions of chromosomes, whose bulk is located in the centre of the nucleus, contact the nuclear periphery (27). This may be especially true of a large chromosome such as HSA1. Similarly, megabase-sized regions of chromatin can loop away from the bulk chromosome territory that is visible with a chromosome paint (28). To address this, a detailed analysis of the nuclear organization of subdomains for individual chromosomes needs to be undertaken. Nevertheless, the information that we have presented here allows us to begin to integrate the primary sequence of the human genome with

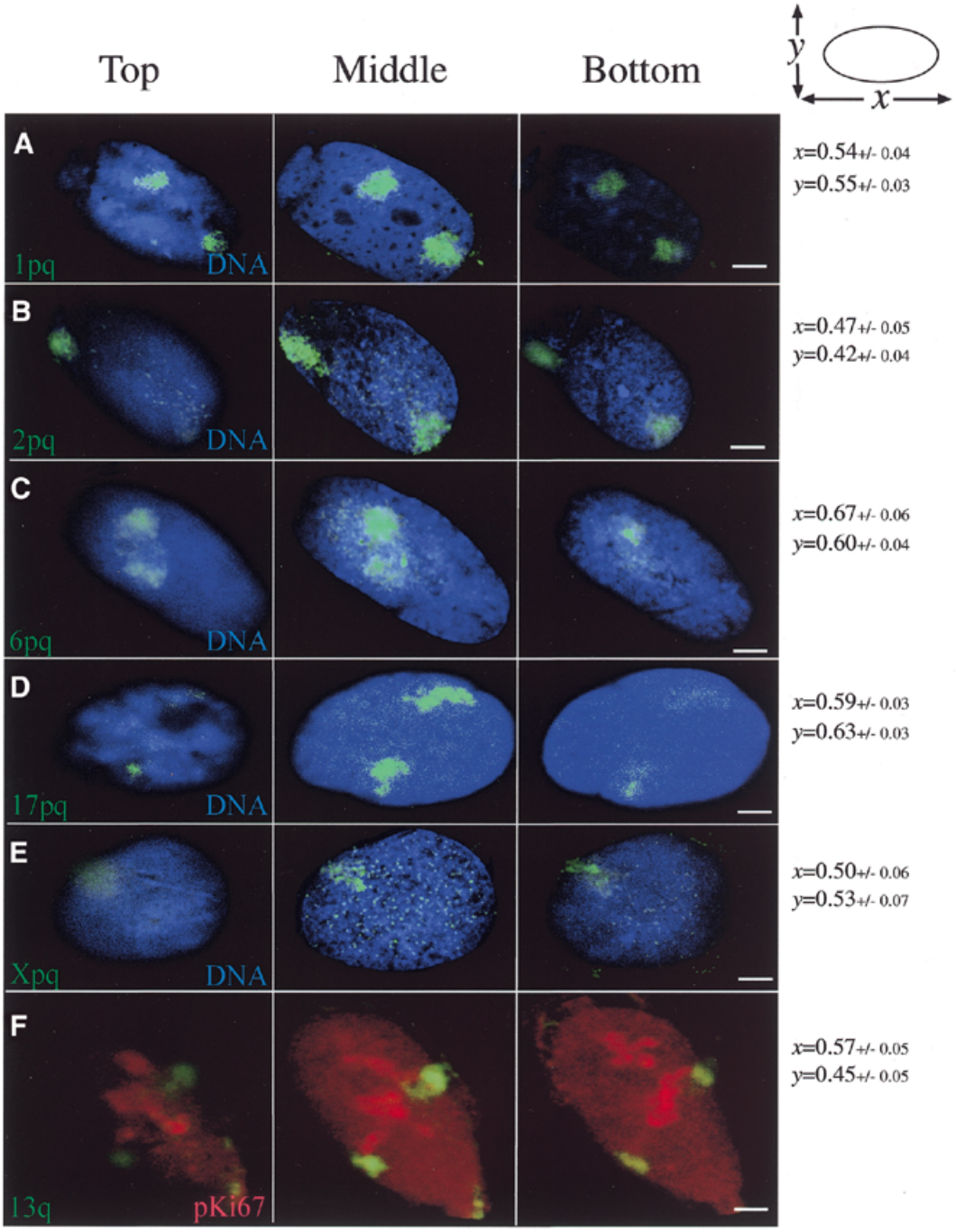

Figure 5. Chromosome position in three-dimensionally preserved nuclei. Selected images (at 2 µm intervals) from the top to the bottom of male fibroblast nuclei fixed in 4% paraformaldehyde. Hybridization signal from chromosomes and chromosome arms (green) is as indicated in each panel. (**A**–**E**) DNA counterstain is shown in blue. In (**F**) immunofluorescence signal from the nucleolar antigen pKi67 (red) is used to show the position of nucleoli. Background signal from this fluorochrome was also used to delineate the nuclear periphery. Mean distances between the centre of each chromosome and the apical (*x*-axis) and lateral (*y*-axis) edges of the nucleus (n = 15–40) are shown as a proportion of the nuclear radius to the right. Bars, 2 µm.

other dimensions of organization that can impact on genome function and dysfunction. Our data can now serve as a basis from which to analyse the position of individual genes.

Nuclear architecture is maintained via protein complexes that span the nuclear envelope. Emerin has been proposed to be part of a novel nuclear protein complex, consisting of at least nuclear lamins A/C and B (10). Recently, the gene for autosomal dominant EDMD was identified as encoding lamin A/C (29). The absence of either emerin or lamin A/C could therefore affect the cellular localization and/or function of the other. It has been reported in X-EDMD (30) and in lamin A-deficient mice (in which emerin fails to locate at the nuclear membrane) (31) that condensed chromatin, usually visible underlying the nuclear envelope, is thin or absent. This has led

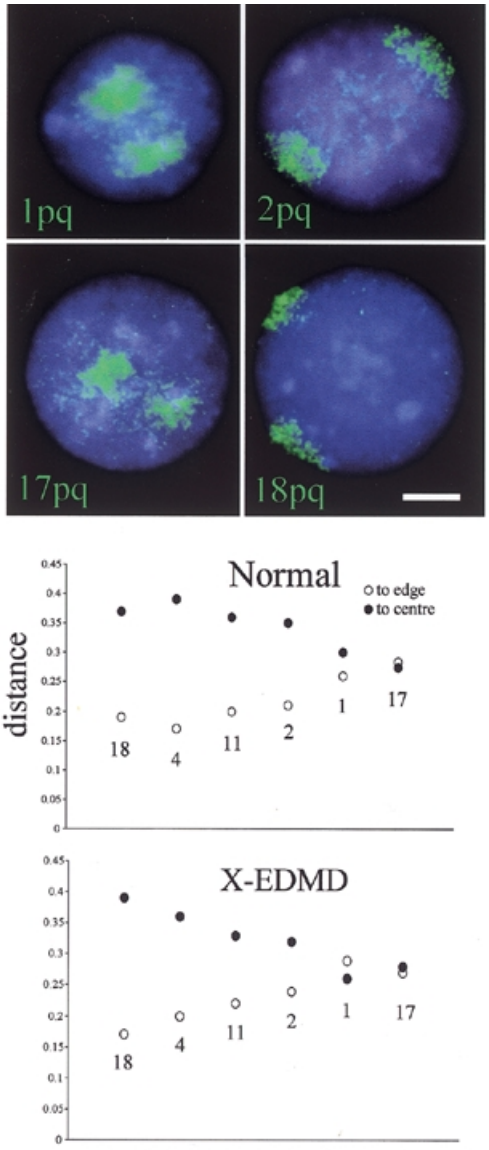

Figure 6. The position of selected chromosome territories in both normal and X-EDMD lymphoblast nuclei. Shown at the top are representative images of selected chromosome territories (green) in nuclei (blue) from individual K2 (21) who has X-EDMD. Bar, 2 μm. Below, graphs compare the normalized mean distances (in pixels) between the centroid of the chromosome territories and either the edge (open circles) or centroid (closed circles) of 50 normal or X-EDMD lymphoblast nuclei each. All standard errors of the mean were ≤0.01.

to the suggestion that a failure to correctly sequester transcriptionally inert chromatin at the nuclear periphery might contribute to the pathology of EDMD by perturbing gene expression (11,32). Emerin belongs to a family of nuclear lamina-associated proteins which includes MAN1 (33) and the lamina-associated polypeptide 2 (LAP2) isoforms, all of which contain a region of homology in their N-terminal region termed the LEM domain. LAP2β interacts with lamin B, chromatin (34) and the DNA-binding protein barrier-to-autointegration factor (BAF) (35). Both the BAF and chromatin binding sites in LAP2β overlap the LEM domain (34). It remains to be established whether BAF is responsible for cross-linking LAP2β to chromatin. Emerin is therefore predicted to bind BAF, providing the necessary link for it to function in organizing chromatin within the nucleus. However, our data show that emerin is not required for anchoring gene-poor chromosomes at the nuclear periphery. If loss of emerin contributes to disease phenotype through a mis-regulation of chromatin organization leading to gene expression changes, it does not operate at the level of nuclear architecture that we have described, or it is cell-type specific.

MATERIALS AND METHODS

Preparation of chromosome painting probes

Chromosome paints were mainly prepared by the amplification of total DNA from micro-dissected p and q arms (7,36). We used q arm paints only for HSA13, -14, -15, -21 and -22 to avoid cross-hybridization between shared p arm sequences. In addition, directly labelled paints for HSA4, -5 and -6 were purchased from Oncor.

FISH and immunofluorescence

Lymphoblastoid cells used were from one normal and one EDMD male. Low passage number fibroblasts used were from one normal female and two different normal males. Fixation of two- and three-dimensional preparations of lymphoblasts and fibroblast cells in 3:1 MAA or 4% paraformaldehyde (PFA) was as previously described (7,12). Briefly, for two-dimensional analysis, lymphoblast or fibroblast cells were swollen in hypotonic medium before fixation in MAA, dropping onto slides and air-drying. For three-dimensional analysis, fibroblast cells, grown directly on microscope slides, were fixed immediately in 4% PFA without swelling in hypotonic medium, then permeabilized prior to FISH (7). Labelled chromosome paint (200 ng) and 10–30 μg of *Cot*I DNA were used per slide. Biotinylated probes were detected using fluorochrome-conjugated avidin [fluorescein isothiocyanate (FITC) or Texas Red] (Vector), followed by biotinylated anti-avidin (Vector) and a final layer of fluorochrome-conjugated avidin. Digoxigenin-labelled probes were detected with sequential layers of FITC-conjugated anti-digoxigenin (BCL) and FITC-conjugated anti-sheep (Vector). Immunofluorescence for the pKi67 antigen was as described by Bridger *et al.* (12).

Slides were counterstained with 0.5 μg/ml 4,6-diamidino-2-phenylindole (DAPI) and examined using a Zeiss Axioplan 2 fluorescence microscope, equipped with a triple band-pass filter (Chroma #83000). Grey-scale images were collected with a cooled charged-coupled device (CCD) camera (Princeton Instruments Pentamax) and analysed using custom IPLab scripts. For three-dimensional analysis a focus motor was used to collect images at 0.5 μm intervals in the *z* direction from a Zeiss Axioplan using a Xillix CCD camera. Some three-dimensional analysis was also performed by confocal scanning laser microscopy as previously described (12).

Image analysis

Scripts described previously (7,12) were used to analyse the data from two-dimensional specimens. In the first, most applicable to spherical nuclei, the area and centroid co-ordinates of the segmented DAPI image were calculated for 50 nuclei. Back-

ground was removed from hybridization signals by subtracting the mean pixel intensity. The area and signal intensity weighted centroid co-ordinates of each segmented signal were calculated and the signal area was normalized by dividing by the nuclear area. The DAPI image was converted to binary form. The nearest edge of the nucleus to the signal was determined by dilating and eroding a segmentation disc from the position of the signal centroid until a single pixel with zero intensity was determined. The signal segment was converted to binary form, a chord was drawn from the centroid of the signal to the nearest edge of the nucleus and the co-ordinates established for the first pixel with zero intensity. This was taken to be the edge of the hybridization signal closest to the nuclear periphery. These co-ordinates were used to determine the relative distances between the weighted centre of the signal and the nearest edge of the nucleus and also between the centre of the signal and the centre of the nucleus. Linear regression analysis between chromosome position and either chromosome size (17) or estimated gene density (1) was performed using Minitab 13.

The erosion script segmented the DAPI signal and recorded the area and centroid co-ordinates. The area was divided into concentric shells (1–5) of equal area from the periphery of the nucleus to the centre. Background was removed from the FISH signal by subtraction of the mean signal pixel intensity within the segmented nucleus. The proportion of FISH signal and DAPI fluorescence was then calculated for each shell of >50 nuclei. The significance of the data was tested by one-way analysis of variance using Minitab 13.

To analyse three-dimensional data, image stacks were deconvolved using PowerHazebuster (VayTek). Distances in pixels/μm between the centre of each chromosome territory and the apical (*x*-axis) and lateral (*y*-axis) edges of the nucleus (as determined from the counterstain) were measured manually as was the nuclear radius across the *x*- and *y*-axes.

ACKNOWLEDGEMENTS

We thank Michael Bittner (Bethesda, MD) for providing us with human chromosome arm paints. We are indebted to Paul Perry (MRC HGU) for customized image capture and analysis scripts. W.A.B. is a Centennial Fellow in Human Genetics of the James S. McDonnell Foundation. S.G. is in receipt of an MRC PhD studentship.

REFERENCES

1. Deloukas, P., Schuler, G.D., Gyapay, G., Beasley, E.M., Soderlund, C., Rodriguez-Tome, P., Hui, L., Matise, T.C., McKusick, K.B., Beckmann, J.S. *et al.* (1998) A physical map of 30 000 human genes. *Science*, **282**, 744–746.
2. Dunham, I., Shimizu, N., Roe, B.A., Chissoe, S., Hunt, A.R., Collins, J.E., Bruskiewich, R., Beare, D.M., Clamp, M., Smink, L.J. *et al.* (1999) The DNA sequence of human chromosome 22. *Nature*, **402**, 489–495.
3. The chromosome 21 mapping and sequencing consortium. (2000) The DNA sequence of human chromosome 21. *Nature*, **405**, 311–319.
4. Brown, K.E., Guest, S.S., Smale, S.T., Hahm, K., Merkenschlager, M. and Fisher, A.G. (1997) Association of transcriptionally silent genes with Ikaros complexes at centromeric heterochromatin. *Cell*, **91**, 845–854.
5. Francastel, C., Ealters, M.C., Groudine, M. and Martin, D. (1999) A functional enhancer suppresses silencing of a transgene and prevents its localization close to centromeric heterochromatin. *Cell*, **99**, 259–269.
6. Andrulis, E.D., Neiman, A.M., Zappulla, D.C. and Sternglanz, R. (1998) Perinuclear localization of chromatin facilitates transcriptional silencing. *Nature*, **394**, 592–595.
7. Croft, J.A., Bridger, J.M., Perry, P., Boyle, S., Teague, P. and Bickmore W.A. (1999) Differences in the localization and morphology of chromosomes in the human nucleus. *J. Cell Biol.*, **145**, 1119–1131.
8. Gruenbaum, Y., Wilson, K.L., Harel, A., Goldberg, M. and Cohen, M. (2000) Nuclear lamins—structural proteins with fundamental functions. *J. Struct. Biol.*, **129**, 313–323.
9. Manilal, S., Recan, D., Sewry, C.A., Hoeltzenbein, M., Llense, S., Leturcq, F., Deburgrave, N., Bardot, J.-C., Man, N.T., Muntoni, F. *et al.* (1998) Mutations in Emery–Dreifuss muscular dystrophy and their effects on emerin protein expression. *Hum. Mol. Genet.*, **7**, 855–864.
10. Fairley, E.A.L., Kendrick-Jones, J. and Ellis, J.A. (1999) The Emery–Dreifuss muscular dystrophy phenotype arises from aberrant targeting and binding of emerin at the inner nuclear membrane. *J. Cell Sci.*, **112**, 2571–2582.
11. Wilson, K.L. (2000) The nuclear envelope, muscular dystrophy and gene expression. *Trends Cell Biol.*, **10**, 125–129.
12. Bridger, J.M., Boyle, S., Kill, I.R. and Bickmore, W.A. (2000) Re-modelling of nuclear architecture in quiescent and senescent human fibroblasts. *Curr. Biol.*, **10**, 149–152.
13. Carothers, A.D. (1999) Projective stereology in biological microscopy. In Baldock, R. and Graham, J. (eds), *Image Processing and Analysis: A Practical Approach.* Oxford University Press, Oxford, UK, pp. 249–260.
14. Craig, J.M. and Bickmore, W.A. (1994) The distribution of CpG islands in mammalian chromosomes. *Nature Genet.*, **7**, 376–382.
15. Saccone, S., de Sario, A., Wiegant, J., Raap, A.K., della Valle, G. and Bernardi, G. (1993) Correlations between isochores and chromosomal bands in the human genome. *Proc. Natl Acad. Sci. USA*, **90**, 11929–11933.
16. Jeppesen, P. (1997) Histone acetylation: a possible mechanism for the inheritance of cell memory at mitosis. *Bioessays*, **19**, 67–74.
17. Morton, N.E. (1991) Parameters of the human genome. *Proc. Natl Acad. Sci. USA*, **88**, 7474–7476.
18. Belmont, A., Bignone, F. and Ts'o, P.O.P. (1986) The relative intranuclear positions of Barr bodies in XXX non-transformed human fibroblasts. *Exp. Cell Res.*, **165**, 165–179.
19. Eils, R., Dietzel, S., Bertin, E., Schröck, E., Speicher, M.R., Reid, T., Robert-Nicoud, M., Cremer, C. and Cremer, T. (1996) Three-dimensional reconstruction of painted human interphase chromosomes: active and inactive X chromosome territories have similar volumes but differ in shape and surface structure. *J. Cell Biol.*, **135**, 1427–1440.
20. Cross, S.H., Clark, V.H., Simmen, M.W., Bickmore, W.A., Maroon, H., Langford, C.F., Carter, N.P. and Bird, A.P. (2000) Preparation and characterisation of CpG island libraries from human chromosomes 18 and 22. *Mamm. Genome*, **11**, 373–383.
21. Ellis, J.A., Craxton, M., Yates, J.R. and Kendrick-Jones, J. (1998) Aberrant intracellular targeting and cell cycle-dependent phosphorylation of emerin contribute to the Emery–Dreifuss muscular dystrophy phenotype. *J. Cell Sci.*, **111**, 781–792.
22. Sadoni, N., Langer, S., Fauth, C., Bernardi, G. Cremer, T., Turner, B.M. and Zink, D. (1999) Nuclear organization of mammalian genomes: polar chromosome territories build up functionally distinct higher order compartments. *J. Cell Biol.*, **146**, 1211–1266.
23. Warburton, D., Naylor, A.F. and Warburton, F.E. (1973) Spatial relations of human chromosomes identified by quinacrine fluorescence at metaphase. *Humangenetik*, **18**, 297–306.
24. Hens, L., Kirsch-Volders, M., Verschaeve, L. and Susanne, C. (1982) The central location of the small and early replicating chromosomes in human diploid metaphase figures. *Hum. Genet.*, **60**, 249–256.
25. Wollenberg, C., Kiefaber, M.P. and Zang, K.D. (1982) Quantitative studies on the arrangement of human metaphase chromosomes IX. Arrangement of chromosomes with and without spindle apparatus. *Hum. Genet.*, **62**, 310–315.
26. Sun, H.B., Shen, J. and Yokota, H. (2000) Size-dependent positioning of human chromosomes in interphase nuclei. *Biophys. J.*, **79**, 184–190.
27. Ferreira, J., Paolella, G., Ramos, C. and Lamond, A.I. (1997) Spatial organization of large-scale chromatin domains in the nucleus: a magnified view of single chromosome territories. *J. Cell Biol.*, **139**, 1597–1610.
28. Volpi, E.V., Chevret, E., Jones, T., Vatcheva, R., Williamson, J., Beck, S., Campbell, R.D., Goldsworthy, M., Powis, S.H., Ragoussis, J. *et al.* (2000). Large-scale chromatin organization of the major histocompatibility complex and other regions of human chromosome 6 and its response to interferon in interphase nuclei. *J. Cell Sci.*, **113**, 1565–1576.

29. Bonne, G., di Barletta, M.R., Varnous, S., Bécane, H.-M., Hammouda, E.-H., Merlini, L., Muntoni, F., Greenberg, C.R., Gary, F., Urtizberea, J.-A. *et al.* (1999) Mutations in the gene encoding lamin A/C cause autosomal dominant EDMD. *Nature Genet.*, **21**, 285–288.
30. Ognibene, A., Sabatelli, P., Petrini, S., Squarzoni, S., Riccio, M., Santi, S., Villanova, M., Palmeri, S., Merlini, L. and Maraldi, N.M. (1999) Nuclear changes in a case of X-linked Emery–Dreifuss muscular dystrophy. *Muscle Nerve*, **22**, 864–869.
31. Sullivan, T., Escalante-Alcalde, D., Bhatt, H., Anver, M., Bhat, N., Nagashima, K., Stewart, C.L. and Burke, B. (1999) Loss of A-type lamin expression compromises nuclear envelope integrity leading to muscular dystrophy. *J. Cell Biol.*, **147**, 913–919.
32. Östlund, C., Ellenberg, J., Hallberg, E., Lippincott-Schwartz, J. and Worman, H.J. (1999) Intracellular trafficking of emerin, the Emery–Dreifuss muscular dystrophy protein. *J. Cell Sci.*, **112**, 1709–1719.
33. Lin, F., Blake, D.L., Callebaut, I., Skerjanc, I.S., Holmer, L., McBurney, M.W., Paulin-Levasseur, M. and Worman, H.J. (2000) MAN1, an inner nuclear membrane protein that shares the LEM domain with lamina-associated polypeptide 2 and emerin. *J. Biol. Chem.*, **275**, 4840–4847.
34. Furukawa, K., Glass, C. and Kondo, T. (1997) Characterization of the chromatin binding activity of lamina-associated polypeptide (LAP) 2. *Biochem. Biophys. Res. Commun.*, **238**, 240–246.
35. Furukawa, K. (1999) LAP2 binding protein (L2BP/BAF) is a candidate mediator of LAP2-chromatin interaction. *J. Cell Sci.* **112**, 2485–2492.
36. Guan, X.Y., Zhang, H., Bittner, M., Jiang, Y., Meltzer, P. and Trent, J. (1996) Chromosome arm painting probes. *Nature Genet.* **12**, 10–11.